A New Calibration Procedure for 3-D Shape Measurement System Based on Phase-Shifting Projected Fringe Profilometry

Rosario Anchini, Giuseppe Di Leo, Consolatina Liguori, *Member, IEEE*, and Alfredo Paolillo, *Member, IEEE*

***Abstract*—An original procedure is presented for the calibration of fringe-projection-based 3-D vision systems. The proposed approach estimates both the phase-to-depth and transverse relationships by directly measuring the phase maps for only three planes placed within the calibration volume and then estimating the phase maps for a number of other "virtual planes." Experimental tests conducted on a fringe projection system show the effectiveness of the proposed procedure.**

***Index Terms*—Calibration, image analysis, lighting, linear approximation, phase measurement, reverse engineering, shape measurement, uncertainty, 3-D scanner.**

I. Introduction

In THE PAST decade, optical 3-D shape measurement systems have been gaining an increasing importance in numerous fields of activities, ranging from the first reverse engineering applications requiring the acquisition of canonical surfaces up to other areas as diverse as industry, health, space exploration, and cultural heritage, to name a few. Today, the industry is very attracted by the possibilities given by the inspection of products performed by optical measurement systems [1]–[3], which capture shape data from surfaces in the form of clouds of points. The contactless inspection of manufactured goods has been successful in different areas, such as the automotive industry, semiconductor inspection, food, and pharmaceuticals manufacturing, where the goal of reducing production costs can be achieved by saving manual labor and limiting defective parts, thus ensuring a consistent product quality. Optical 3-D shape measurement systems can also allow manufacturers to check goods (silicon wafers, semiconductor chips, or surfaces of painted vehicles) one by one for defects, with the aim of controlling the parameters of the industrial process as soon as a defect is found. On the other hand, the current tendency evolves toward the use of scanners in the reconstruction of human faces, sculptures, paintings, prehistorical footprints, etc. The key to their success can be found in their distinctive attributes. Indeed, flexibility, reliability, higher operating speeds, consistency, and objectivity have made them competitive with respect to traditional measurement systems.

Manuscript received June 30, 2008; revised December 18, 2008. First published February 6, 2009; current version published April 7, 2009. The Associate Editor coordinating the review process for this paper was Dr. Emil Petriu.

The authors are with the Department of Electrical and Information Engineering (DIIIE), University of Salerno, 84084 Salerno, Italy (e-mail: ranchini@unisa.it; gdileo@unisa.it; tliguori@unisa.it; apaolillo@unisa.it).

Color versions of one or more of the figures in this paper are available online at http://ieeexplore.ieee.org.

Digital Object Identifier 10.1109/TIM.2009.2012952

Shape acquisition can be accomplished in several ways. A widely adopted solution is based on fringe projection systems, which are composed of a camera and a projection unit. Such systems relate each surface point to three coordinates (x, y, and z) expressed in a given 3-D coordinate system that usually has the z-axis orthogonal to a given reference plane. The operation of such systems is based on the measurement of the spatial phase, as seen by the camera when a sequence of periodic light intensity patterns is projected onto the scene. The phase measurement is performed on the reference plane during the calibration and then on the object under analysis during the measurement phase. Eventually, the 3-D coordinates of a large set of points are achieved by processing the phase maps.

Regardless of the chosen method, the calibration of a vision-based measurement system is a critical task. This stage is always preliminary at any measurement since it evaluates the vision system parameters that are necessary to infer 3-D information from the 2-D images acquired by the camera. The calibration stage has been the subject of a large number of works over the years, due to its impact on the overall accuracy of the final measurements [4]–[8]. As an example, to monitor the conservation status of a sculpture, even micrometric changes in any point of the surface could be relevant. For these reasons, the uncertainty of 3-D scanner measurements must be suitably low with respect to the resolution required by the application.

On the other hand, many acquisition tasks must be carried out on-site and often within a limited amount of time. This could be the case of acquisition campaigns of heritage sites or crime scene analysis, for instance. In these situations, a fast and easy-to-use calibration solution is strongly required to allow moving the scanner devices into different positions to cover the whole site or the whole work of art. Furthermore, the field of view of the scanning system often has to be changed through modifications in the relative positions of the camera and the projector to adapt it to the surface under analysis [9]. The various imaged sights (patches) have to overlap to register them into a single consistent cloud of points. After each single change in position and optical configuration, the system has to be recalibrated. This may happen several times during a single acquisition campaign. To better fulfill all these requirements in practical applications, a tradeoff between the processing time and uncertainty of measurement results is worth a dedicated research activity since currently adopted calibration approaches, such as those described in [4]–[10], do not often comply with the time constraints of the application.

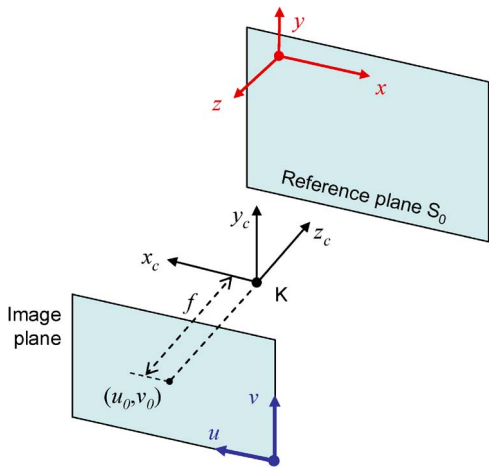

Fig. 1. Definition of the coordinate systems.

This paper is an extension of a previous paper [11], where the authors introduced an original method for calibrating fringe-projection-based 3-D vision systems with three aims.

1) Affordable and easy to implement: The equipment intended to be used specifically for calibration purposes should have a low impact on the cost of the whole system hardware and should not be cumbersome to use on a site outside of the laboratory.
2) Time saving: The proposed calibration leads in every session at the acquisition of a small number of images.
3) Accurate: The method implicitly takes into account the distortions of both the projection and the imaging optics, as other known calibration procedures do.

In the following, after a brief recall of the most widespread calibration approaches, the proposed procedure is presented, highlighting its original aspects; finally, the first experimental results are reported.

II. Calibration of Fringe Pattern Scanners: State of the Art

In fringe projection systems for 3-D reconstruction, a sequence of periodic light intensity patterns is projected onto the reference plane and then on the measuring object. Then, processing the acquired images with the projected fringe on the object, the three coordinates (x, y, and z) of the object under measurement, which are expressed in a given 3-D coordinates system having the z-axis orthogonal to reference plane S_0, are obtained. Fig. 1 shows the different coordinate systems involved in the camera model: the absolute 3-D coordinate system (x, y, and z), the camera coordinate system (x_c, y_c, z_c) centered at the camera projection center and the pixel coordinate system (u, v) defined on the camera sensor plane. The so-called principal point is defined as the intersection (u_0, v_0) between the sensor plane and the camera axis. The length f between the origin K of the camera coordinate system and the sensor plane is the so-called camera constant.

After the projection of a sinusoidal pattern (see, e.g., Fig. 2) on a reference plane, the light intensity $I_{\mathrm{Ref}}(u, v)$ acquired as a digital image by the camera spatially varies with respect to pixel location (u, v). By analogy with the case of time-domain signals, one can introduce the spatial period of fringes (expressed in pixels) and the spatial frequency (in pixels^{-1}) and spatial phase (in radians). This way, the spatial variation of the acquired spatial intensity $I_{\mathrm{Ref}}(u, v)$ can be seen as a sinusoidal variation modulated by terms due to the perspective and the surface location. Following a common approach, the modulation terms can be quantified through the analysis of the spatial phase on the digital image by running specific algorithms [6], [12], [13]. The interest in measuring phase values during the calibration is motivated by the idea that, after the calibration, one can exploit analytical or empirical relationships between the observed spatial phase and the depth (namely, the absolute z coordinate) of each point of an unknown illuminated surface under analysis. Phase values $\varphi(u, v)$ at pixel image location (u, v) can be achieved through a phase-shifting method [12], [13] that requires the projection of a small number (at least three) of N_{pattern} sinusoidal patterns, each having a phase shifted by $2\pi/N_{\mathrm{pattern}}$ with respect to the previous pattern. These algorithms are run to measure both the spatial phase $\varphi_{\mathrm{ref}}(u, v)$ on one or more reference planes during the calibration and the $\varphi_{\mathrm{obj}}(u, v)$ on an unknown surface under analysis (located within the volume identified during the calibration) during a measurement task. $\varphi_{\mathrm{ref}}(u, v)$ acts as a common phase reference, and the difference between the two phase maps $\Delta\varphi(u, v) = \varphi_{\mathrm{obj}}(u, v) - \varphi_{\mathrm{ref}}(u, v)$ can be related to the height $z(u, v)$ of the surface point imaged at pixel (u, v) with respect to the reference plane.

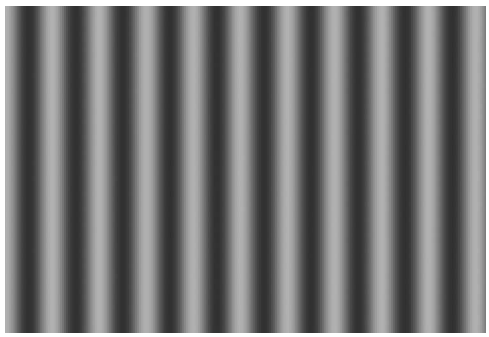

Fig. 2. Example of the sinusoidal pattern.

The retrieval of depth z as a function of the spatial phase, when a reference plane is illuminated, is just the first step of the whole calibration. In particular, it can be outlined in two main steps [6].

1) The longitudinal calibration finds the phase-to-depth relationship between the z coordinate of each surface point imaged at pixel (u, v) and the phase $\varphi(u, v)$, i.e.,

$$z = f_z\left(\varphi_{\mathrm{ref}}(u, v)\right). \tag{1}$$

2) The transverse calibration determines the two functional forms relating the transverse absolute coordinates x and y of each surface point imaged at pixel (u, v) to $\varphi(u, v)$, i.e.,

$$\begin{aligned} x &= f_x\left(\phi_{\mathrm{ref}}(u, v)\right) \\ y &= f_y\left(\phi_{\mathrm{ref}}(u, v)\right). \end{aligned} \tag{2}$$

In the literature, several solutions are known for the definition of the functionals in (1) and (2) for fringe projection systems,

but the approaches more commonly used can be classified as analytical [4], [8] or empirical [5]–[7], [11]. In particular, the calibration methods of the former class derive mathematical expressions for both the phase-to-depth and transverse relationships. They rely on a precise determination of geometrical distances, such as camera and projection locations in the 3-D space, which appear as parameters in the functions f_x, f_y, and f_z in (1) and (2). However, even the smallest change between the projecting and the imaging unit results in measurement errors, which are relevant in measurement applications. Moreover, they do not explicitly account for the distortions of both the projection and the imaging optics. Neglecting the aberrations severely impacts the final results [14].

On the other hand, some calibration methods [5]–[7] empirically evaluate the phase-to-depth and transverse functionals. They adopt a parametric nonlinear expression for relationships f_x, f_y, and f_z. Given a pixel (u, v), the unknown coefficients of f_x, f_y, or f_z can be calculated through the interpolation of N phase values measured at pixel (u, v) when the acquired flat reference plane successively translates to N different and known depth positions. Although corrective coefficients accounting for various distortions can be added to the parametric equations to improve the accuracy of the approximation, the performance of the "empirical" methods depends on the accuracy of the traveling stage moving the reference plane, which makes scanning campaigns outside of the laboratory fairly intricate. Moreover, they appear to be more time consuming than the "analytical" calibration procedures. The proposed approach follows an "empirical" strategy to find out the parameters of both the phase-to-depth relationship (1) and the two transverse functional forms (2). The two calibration tasks of the proposal are the subjects of the two succeeding sections.

III. Longitudinal Calibration

The "empirical" strategy for the phase-to-depth relationship allows one to achieve a low uncertainty on the coordinate measurements of the surface points [6]. Even though its development has collected some suggestions from known calibration methods, the authors propose original aspects. The authors noticed that the number N of the necessary phase maps to be acquired at different reference plane locations during calibration can drastically be reduced with respect to consolidated "empirical" strategies by exploiting some well-founded assumptions described here. As previously stated, the longitudinal calibration is usually achieved by successively translating a flat surface to N different depth positions until the whole calibration volume is covered. Since the smaller the step size, the better the performance of the measurement system, several positions have to be imaged by the camera. In the proposed approach, the plane surface has to be moved into only three different positions, as shown in Fig. 3. The three poses of the plane must be chosen such that the volume where the surface to be acquired will lie is bounded by the nearest (S_0) and farthest (S_1) parallel poses of the plane, and the intersection lines between S_0 and the slanted plane S_2 and those between S_1 and S_2 fall within the field of view of the camera. The angle of rotation of the S_2 plane should be chosen according

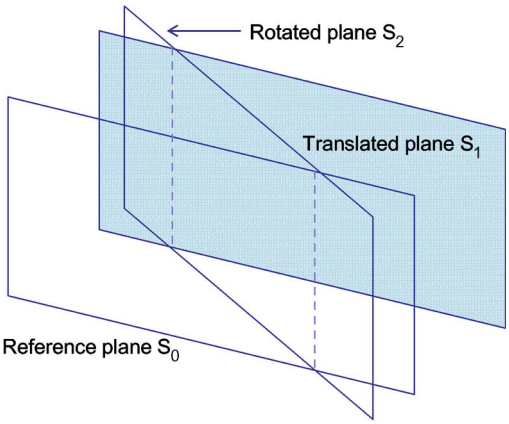

Fig. 3. Positions of the flat surface for the longitudinal calibration.

to the suggestions in [7], but an exact knowledge of its value is not necessary. In the practical experiments reported here, it has been set approximately equal to 20°.

According to the proposed procedure, the distribution of the absolute phase on the flat surface is measured on each of the three planes S_0, S_1, and S_2 through a traditional algorithm, such as a phase-shifting algorithm, yielding phase maps $\varphi_{0r}(u, v)$, $\varphi_{1r}(u, v)$, and $\varphi_{2r}(u, v)$, respectively. The idea is to process these phase maps by exploiting proper assumptions to estimate the phase map $\varphi_v(u, v)$ of any plane S_v located within the calibration volume. Each function $\varphi_v(u, v)$ is hereinafter called the virtual map associated with a corresponding virtual plane S_v. The adjective "virtual" highlights that S_v is not really placed into the 3-D space during the calibration session but that its absolute virtual map is indirectly calculated by using $\varphi_{0r}(u, v)$, $\varphi_{1r}(u, v)$, and $\varphi_{2r}(u, v)$. The proposed calibration approach is based on three observations.

1) The plausible working conditions of a fringe projection measurement system determine a region of interest along the actual phase-to-depth curve where the relationship between the z coordinate of each surface point imaged at pixel (u, v) and the phase $\varphi(u, v)$ can be approximated as linear [7], i.e.,

$$z(x, y) = \varepsilon + \lambda \cdot \Delta\phi(x, y). \tag{3}$$

2) Given a generic plane surface S_v parallel to the reference plane surface S_0, with D being the distance between S_v and S_0, as shown in Fig. 4, it can be demonstrated through geometrical considerations that the function $\Delta\varphi$ into plane S_v is given by the following:

$$\begin{aligned}\Delta\varphi &= 2\pi f_0 \left\{\overline{OO'} - [\overline{OB} + \overline{OB'}]\right\} \\ &= 2\pi f_0 \left\{\left[\overline{KP} - L_p \cos\left(\frac{\pi}{2} - \alpha\right) - L_p \sin\left(\frac{\pi}{2} - \alpha\right) \tan(\beta)\right] \right. \\ &\quad \cdot [\cos(\alpha - \gamma') + \sin(\alpha - \gamma') \tan(\beta + \alpha - \gamma')] \\ &\quad + - \left[\overline{AO''} \frac{L_k}{L_k + \frac{D}{\cos(\gamma)}} - \overline{A'O''} \frac{L_p}{L_p + \frac{D}{\cos(\gamma')}} \right. \\ &\quad \left. \left. - x \left(\frac{L_k}{L_k + \frac{D}{\cos(\gamma)}} - \frac{L_p}{L_p + \frac{D}{\cos(\gamma')}} \right) \right] \right\}\end{aligned} \tag{4}$$

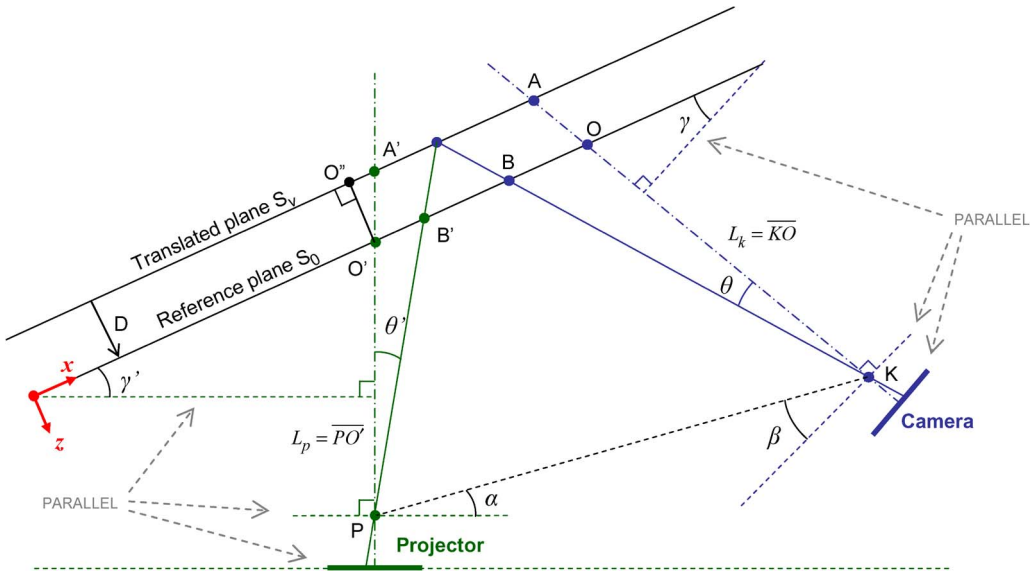

Fig. 4. Geometrical configuration for the definition of the general phase-x (4).

where f_0 is the fringe spatial frequency; L_p and L_k are the distances between the projection center P of the projector and the projection center K of the camera, respectively; γ and γ' are the angles between the reference plane and the camera sensor plane and the projector grid plane, respectively; β and α are the angles between the KP baseline and the camera sensor plane and the projector grid plane, respectively; A is the intersection between the projector axis and S_1; A' is the intersection between the camera axis and S_1; and O'' is the intersection between S_1 and the line orthogonal to S_1 through O'. The first three terms in the relationship are constant with respect to x on plane S_1 for a given displacement between the camera and the projection unit. Instead, the fourth term causes quantities $\Delta\varphi$ to linearly vary with respect to the coordinate x taken along an axis parallel to S_1. Thus

$$\Delta\phi = \text{const} + 2\pi f_0 \left(\frac{L_p}{L_p + \frac{D}{\cos(\gamma)}} - \frac{L_k}{L_k + \frac{D}{\cos(\gamma')}} \right) \cdot x. \quad (5)$$

3) The coordinates (x_2, y_2, z_2) of a point P on a rotated plane S_2 can be expressed in the coordinates system of the reference plane S_0 through the following transformation [7] (see Fig. 5):

$$\begin{pmatrix} x_0 \\ y_0 \\ z_0 \end{pmatrix} = \text{Tr}_{0C}^{-1} \text{Tr}_{2C} \begin{pmatrix} x_2 \\ y_2 \\ z_2 \end{pmatrix} \quad (6)$$

where rototranslation matrix Tr_{0C} describes the transformation from the coordinate system of S_0 to the camera reference system (x_c, y_c, z_c) shown in Fig. 1, and matrix Tr_{2C} describes the rototranslation from the coordinate system integral with the rotated plane S_2 to the coordinate system of the camera (x_c, y_c, z_c). Both matrices are related to the extrinsic parameters of the camera (see Fig. 4) that are estimated with the method proposed in [7].

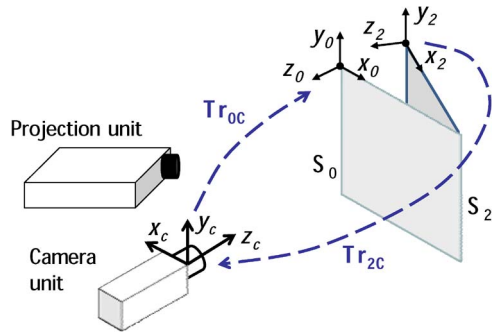

Fig. 5. Transformation from (x_2, y_2, z_2) to (x_0, y_0, z_0) through the camera coordinates.

The procedure starts by calculating the wrapped phase maps $\Delta\varphi_{0w}$, $\Delta\varphi_{1w}$, and $\Delta\varphi_{2w}$ relating to the three planes S_0, S_1, and S_2 through a traditional algorithm, such as the phase-shifting algorithm. Then, these wrapped phase maps are unwrapped through an adaptive integration method [15], obtaining the unwrapped phase maps $\Delta\varphi_0$, $\Delta\varphi_1$, and $\Delta\varphi_2$, respectively. The obtained maps must be coherent, i.e., given any point belonging to the intersection between planes S_i and S_{i+1} and imaged at pixel (u, v), the phase maps associated with these planes are coherent if $\Delta\varphi_{iw}(u, v) = \Delta\varphi_{(i+1)w}(u, v)$.

The coherence for $\Delta\varphi_0$ and $\Delta\varphi_2$ is achieved by choosing a pixel lying on the intersection between S_0 and S_2 as the starting point of the unwrapping algorithm for $\Delta\varphi_{0w}$ and $\Delta\varphi_{2w}$, respectively. Analogously, a pixel lying on the intersection between S_1 and S_2 is selected as the starting point for unwrapping $\Delta\varphi_{1w}$ to obtain $\Delta\varphi_1$. However, this choice does not imply coherence between $\Delta\varphi_2$ and $\Delta\varphi_1$, because a different phase reference value has already been set for $\Delta\varphi_2$. Therefore, $\Delta\varphi_1$ is iteratively shifted by a multiple of 2π at each step until $\Delta\varphi_1(u, v)$ and $\Delta\varphi_2(u, v)$ are equal at a pixel lying on the intersection between S_1 and S_2.

The obtained phase maps allow the estimation of any virtual map. The phase $\Delta\varphi^*(u, v)$ associated with a virtual plane S_v parallel to reference S_0 can be evaluated through two linear

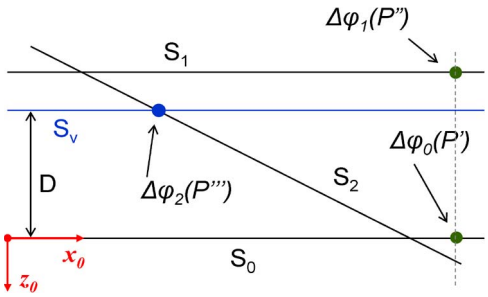

Fig. 6. Calculation of the phase map for a virtual plane.

interpolations involving $\Delta\varphi_0(u_0, v_0)$ with $\Delta\varphi_1(u_1, v_1)$ and then the obtained result with $\Delta\varphi_2(u_2, v_2)$ (see Fig. 6), where two conditions hold.

- (u_0, v_0) and (u_1, v_1) are the locations of the pixels corresponding to points P' and P'' having the same world coordinate x_0.
- (u_2, v_2) is the location of the pixel corresponding to a point P''' of the intersection between S_2 and S_V.

Then, the phase-to-depth relationship can be estimated by adopting the methodology proposed in [6], where virtual phase maps replace the measured maps within the calibration volume.

IV. Transverse Calibration

The transverse calibration can be achieved through the procedure reported in [6], which is based on the following expressions holding for the functional forms (2) at each pixel location (u, v):

$$\begin{aligned} x &= f_x(u, v, z) = a_1(u, v) \cdot z + a_0(u, v) \\ y &= f_y(u, v, z) = b_1(u, v) \cdot z + b_0(u, v) \end{aligned} \tag{7}$$

where the four unknown parameters depend on the chosen location (u, v). All the surface points (x, y, z) imaged to a fixed pixel (u, v) lie on a straight line, which is usually called the line of sight of the pixel. Then, the purpose of the longitudinal calibration becomes to determine the four parameters for each pixel location (u, v). The approach in [6] seems to be laborious since two sinusoidal gratings with their fringes parallel to the x_0- and y_0-directions are sequentially placed in a plane situated at depth z. Assembling the images of these temporally separated but spatially overlapped gratings yields a virtual grid pattern, which serves as a metric standard in the transverse calibration. When a number of virtual grids are successively generated and measured at different depth positions, the lines of sight of different pixels are traced out. Two fringes in the respective gratings are specially marked. The intersection point of these fringes in the virtual grid represents the origin of the x_0y_0 plane.

The authors propose calculating the four parameters for each pixel location (u, v) by simultaneously solving (7) for only two points $P_0(x_0, y_0, 0)$ and $P_1(x_1, y_1, z_{\text{Max}})$ lying on the line of sight of the same pixel (u, v), thus simplifying the methodology in [6]. In particular, points P_0 and P_1 belong to the nearest (S_0) and farthest (S_1) planes bounding the calibration volume, respectively, i.e.,

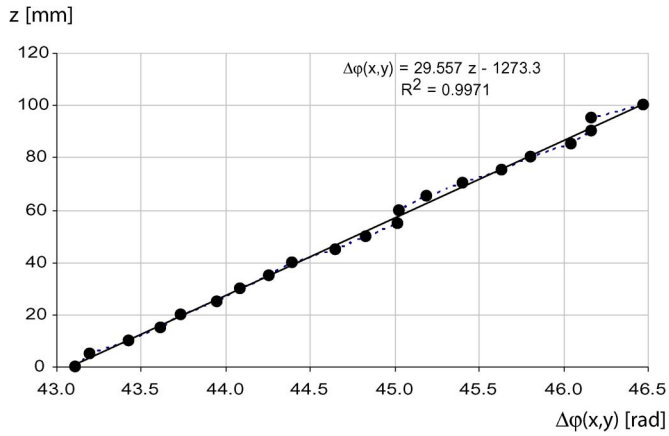

Fig. 7. Experimental phase-to-depth relationship measured on planes at different z's at the same (x, y) coordinates. The equation of the least square line and the R^2 value is shown.

$$\begin{aligned} a_0(u, v) &= x_0 \\ b_0(u, v) &= y_0 \\ a_1(u, v) &= (x_1 - x_0)/z_{\text{Max}} \\ b_1(u, v) &= (y_1 - y_0)/z_{\text{Max}}. \end{aligned} \tag{8}$$

The coordinates of point P_0 expressed into the world reference system can be achieved by considering the following well-known transformation [16]:

$$\begin{aligned} u_{P_0} &= -f \cdot k_u \frac{r_{11}x_0 + r_{12}y_0 + t_x}{r_{31}x_0 + r_{32}y_0 + t_z} + u_0 \\ v_{P_0} &= -f \cdot k_v \frac{r_{21}x_0 + r_{22}y_0 + t_y}{r_{31}x_0 + r_{32}y_0 + t_z} + v_0. \end{aligned} \tag{9}$$

Here, (u_{P_0}, v_{P_0}) is the pixel location corresponding to point P_0. fk_u, fk_v, u_0, and v_0 are related to the intrinsic parameters of the camera that are estimated through the method proposed in [16], where f is the camera constant, k_u and k_v are the reciprocals of the sizes of the pixel areas (in pixels per millimeter) on the camera sensor plane along the u and v coordinate directions (see Fig. 1), respectively, and (u_0, v_0) is the camera principal point. Analogous equations hold for P_1. Then, the values chosen for x_0, y_0, and z_0, and x_1, y_1, and z_1 are those that make u_{P_0} and v_{P_0} equal to u_{P_1} and v_{P_1}, respectively.

V. Experimental Result

A. Experimental Estimation of the Phase-to-Depth Relationship

Prior to evaluating the performances of the proposed system, tests were carried to assess the validity of the hypothesis that the phase-to-depth relationship can be approximated by the linear equation (3) in plausible operating conditions. To this aim, the absolute phase on a reference plane at different depths z was measured, and its values were plotted at the same absolute coordinates (x, y), which are identified with proper markers on the reference plane moving along z. An example of the result is shown in Fig. 7. The good agreement of experimental data

TABLE I
COMPARISON OF ERRORS ALONG THE z COORDINATE

Classic longitudinal calibration (z_{Max}= 50mm)			
D [mm]	Max [mm]	Mean [mm]	Standard dev. [mm]
5	0.8	0.01	0.26
30	0.8	0.01	0.23
45	1.4	0.01	0.52
Linear longitudinal calibration (z_{Max}= 50mm)			
D [mm]	Max [mm]	Mean [mm]	Standard dev. [mm]
5	2.5	1.21	0.50
30	4.8	1.27	1.49
45	6.6	2.52	1.70
Proposed longitudinal calibration (z_{Max}= 50mm)			
D [mm]	Max [mm]	Mean [mm]	Standard dev. [mm]
5	1.6	0.36	0.55
30	1.8	0.19	0.58
45	1.6	0.11	0.48

with a linear model is confirmed by the value of the coefficient of determination R^2 given by [17]

$$R = \frac{n\sum(\Delta\theta \cdot z) - \sum(\Delta\theta)\sum(z)}{\sqrt{\left[n\sum(\Delta\theta^2) - \left(\sum\Delta\theta\right)^2\right]\left[n\sum(z^2) - \left(\sum z\right)^2\right]}} \quad (10)$$

where n is the number of points. The behavior of Fig. 7 is similar throughout the whole reference plane. The plot of the values of phase versus the x coordinate also shows good linear behavior. The adopted geometrical configuration was such that the projector was frontally oriented toward the plane at a distance of about 1 m, and the camera was placed on the left of the projector at a distance of nearly 30 cm.

B. Evaluation of the Accuracy of the Proposed System

Then, a preliminary comparison of the performance between the proposed procedure and the two widespread procedures has been carried out. The other two procedures considered in the comparison are that suggested by Liu *et al.* [6] (called "classical" hereinafter) and that by Tavares and Vaz [7] (called "linear longitudinal" hereinafter). The analysis has involved the use of a 3-D fringe projection scanner that has been developed "ad hoc" and is based on a phase-shifting method [12], [13] with five periodic intensity patterns. Fig. 2 shows one of the adopted patterns that exhibit a period of 30 pixels. The system setup consists of a charge-coupled-device camera with a focal length of 24 mm and a digital-micromirror-device fringe projection unit that offers maximum resolutions of 640 × 480 and 1024 × 768 pixels, respectively.

In the first series of experimental tests, a flat surface parallel to the reference plane has been positioned at a known imposed distance D within the calibration volume measuring less than about 100 mm × 100 mm × 50 mm. Theoretically, all the points of the surface should have the same value for their z coordinates. For this reason, a statistical processing of the differences between D and the z coordinates measured by the scanner, for all the points on the flat surface, can be used for estimating bias and uncertainties along z. Table I reports the mean and maximum values of the differences for the points on a plane, at three different poses (5, 30, and 45 mm) and for the three considered longitudinal calibration procedures. The results from Table I confirm the effectiveness of the proposed procedure. In particular, both the standard deviation and maximum errors are comparable with the results achieved by the classical method, whereas worse behavior is exhibited in terms of mean errors. Moreover, the proposed method shows satisfactory improvements with respect to the performance of the linear approach.

A second series of tests concerned the comparison between the proposed scanner and a reference instrument, i.e., a FARO "Titanium Arm" mod. N06, provided with a laser line probe (single point accuracy: ±53 μm, depth of field: 85 mm). Two clouds of points were acquired with the two instruments from the same object under measurement (a cup). Fig. 8 shows the two clouds of points acquired by the two instruments. The two clouds of points were imported into a 3-D processing software environment (PolyWorks), where a truncated cone was fitted onto the points. The points of the cloud measured by the reference instrument have a higher density, hence assuring better accuracy of the results that have to be used in estimating reference values. Three linear lengths were measured on the truncated cone, and some statistics were calculated. The results are superimposed on Fig. 8 and reported in Table II. They show systematic effects on the order of 1.4% and standard deviations of fitting errors that are just four times greater than those of the reference system.

VI. CONCLUSION

This paper has described a procedure for the calibration of a fringe projection 3-D scanner that exhibits some advantages with respect to other known approaches. It is advantageous in that it requires a plane to be illuminated and imaged in only three poses, whereas a classical approach requires a

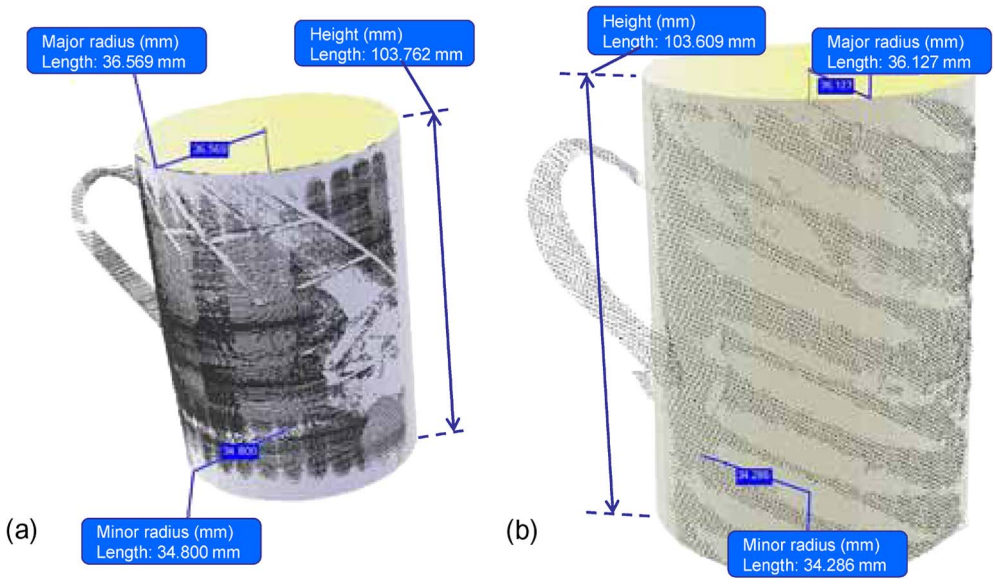

Fig. 8. (Black dots) Two clouds of points acquired by (a) the reference 3-D scanner and (b) the proposed scanner. The labels indicate the measurements of the lengths defined on the fitting truncated cone.

TABLE II
RESULTS OF THE COMPARISON BETWEEN A REFERENCE 3-D SCANNER AND THE PROPOSED SYSTEM

	Proposed	*Reference*	*Error (Proposed – Reference)*
Number of points	32000	183000	---
Major radius	36.569 mm	36.127 mm	0.442 mm (1.2%)
Minor radius	34.800 mm	34.286 mm	0.514 mm (1.4%)
Height	103.762 mm	103.609 mm	0.153 mm (1.4%)
Average of Fitting errors	-10^{-10} mm	$2 \cdot 10^{-11}$ mm	---
Standard deviation of fitting errors	0.94 mm	0.25 mm	---

higher number of poses. Furthermore, the three poses could be obtained without a motorized traveling stage, realizing a specific support that can also be used in an outdoor environment different from a laboratory. The equipment necessary for the calibration (the reference plane and its support) does not significantly contribute to the cost of the whole system. The elaboration times of the proposed procedure are significantly shorter than those of the classical procedure due to the reduced number of images for processing. On the other hand, the achievable accuracy of the presented system is better than that of the "linear longitudinal" calibration. For these reasons, the proposed method can be viewed as a compromise between a lengthy and accurate classical calibration method and a fast but less-accurate "linear longitudinal" method, in terms of accuracy and required times. The comparison with an expensive reference 3-D scanner has showed quite good performances.

REFERENCES

[1] A. M. Wallace, "Industrial applications of computer vision since 1982," *Proc. Inst. Elect. Eng.—Comput. Dig. Techn.*, vol. 135, no. 3, pp. 117–136, May 1988.

[2] Y. Sumi, M. Sallinen, M. Sirvio, and J. Vainola, "Recognition of large work objects in difficult industrial environments," in *Proc. IEEE Int. Conf. Syst., Man Cybern.*, 2004, vol. 6, pp. 5285–5289.

[3] R. Anchini, G. Di Leo, C. Liguori, and A. Paolillo, "New measurement techniques for the on line dimension characterization of automotive rubber profiles," in *Proc. 18th IMEKO World Congr., Metrology Sustainable Develop.*, Rio de Janeiro, Brazil, Sep. 2006.

[4] L. Chen and C. Liao, "Calibration of a 3D surface profilometry using digital fringe projection," *Meas. Sci. Technol.*, vol. 16, no. 8, pp. 1554–1566, Aug. 2005.

[5] Z. Xiaoling, L. Yuchi, Z. Meirong, N. Xiaobing, and H. Yinguo, "Calibration of a fringe projection profilometry system using virtual phase calibrating model planes," *J. Opt. A, Pure Appl. Opt.*, vol. 7, no. 4, pp. 192–197, Apr. 2005.

[6] H. Liu, W. Su, K. Reichard, and S. Yin, "Calibration-based phase-shifting projected fringe profilometry for accurate absolute 3D surface profile measurement," *Opt. Commun.*, vol. 216, no. 1–3, pp. 65–80, Feb. 2003.

[7] P. J. Tavares and M. A. Vaz, "Linear calibration procedure for the phase-to-height relationship in phase measurement profilometry," *Opt. Commun.*, vol. 274, no. 2, pp. 307–314, Jun. 15, 2007.

[8] R. Legarda-Saenz, T. Bothe, and W. P. Juptner, "Accurate procedure for the calibration of a structured light system," *Opt. Eng.*, vol. 43, no. 2, pp. 464–471, Feb. 2004.

[9] G. Guidi, M. Pieraccini, S. Ciofi, V. Damato, J.-A. Beraldin, and C. Atzeni, "Tridimensional digitizing of Donatello's Maddalena," in *Proc. Int. Conf. Image Process.*, Thessaloniki, Greece, Oct. 7–10, 2001, vol. 1, pp. 578–581.

[10] G. Sansoni, S. Lazzari, M. Carocci, and F. Docchio, "Development and characterization of a 3D measuring system based on integration of gray code and phase-shift light projection," in *Proc. SPIE Three-Dimensional Image Capture*, R. N. Ellson and J. H. Nurre, Eds, San Jose, CA, Feb. 11, 1997, pp. 139–147.

[11] R. Anchini, C. D'Argenio, C. Liguori, and A. Paolillo, "An easy and accurate calibration procedure for 3-D shape measurement system based

on phase-shifting projected fringe profilometry," in *Proc. IEEE I2MTC*, Victoria, BC, Canada, May 12–15, 2008, pp. 2044–2049.
[12] Y. Surrel, "Design of algorithms for phase measurement by the use of phase stepping," *Appl. Opt.*, vol. 35, no. 1, pp. 51–60, Jan. 1996.
[13] K. Creath, "Comparison of phase-measurement algorithms," in *Proc. SPIE Surface Characterization Testing*, K. Creath, Ed., Bellingham, WA, 1986, vol. 680, pp. 19–28.
[14] Z. Zhang, D. Zhang, and X. Peng, "Performance analysis of a 3D full-field sensor based on fringe projection," *Opt. Lasers Eng.*, vol. 42, no. 3, pp. 341–353, Sep. 2004.
[15] J. Strand and T. Taxt, "Two-dimensional phase unwrapping using robust derivate estimation and adaptive integration," *IEEE Trans. Image Process.*, vol. 11, no. 10, pp. 1192–1200, Oct. 2002.
[16] Z. Zhang, "A flexible new technique for camera calibration," *IEEE Trans. Pattern Anal. Mach. Intell.*, vol. 22, no. 11, pp. 1330–1334, Nov. 2000.
[17] D. S. Moore and G. P. McCabe, *Introduction to the Practice of Statistics*. San Francisco, CA: Freeman, 2006.

Rosario Anchini was born in Salerno, Italy, in 1976. He received the M.S. degree in electronic engineering and the Ph.D. degree in information engineering from the University of Salerno in 2003 and 2006, respectively.

He is currently with the Department of Electrical and Information Engineering (DIIIE), University of Salerno. His current research interests include systems for noncontact measurement based on image processing, particularly their metrological characterization, with the aim of providing analytical methods to predict the uncertainty of the results of such systems.

Giuseppe Di Leo was born in Sarno (SA), Italy, in 1972. He received the M.S. degree in electronic engineering from the University of Salerno, Salerno, Italy, in 2001. He is currently working toward the Ph.D. degree in information engineering with the University of Salerno.

Since 2002, he has been with the Department of Electrical and Information Engineering (DIIIE), University of Salerno. He has coauthored papers in national and international conference proceedings and journals. His research interests include metrological characterization of measurement systems, image-based measurement systems, and digital signal processing.

Consolatina Liguori (M'99) was born in Solofra (AV), Italy, in 1969. She received the M.S. degree in electronic engineering from the University of Salerno, Salerno, Italy, in 1993 and the Ph.D. degree from the University of Cassino, Cassino, Italy, in 1997.

In 1997, she was an Assistant Professor of electrical measurements with the Department of Industrial Engineering, University of Cassino. In 2001, she became an Associate Professor of electrical and electronic measurements. In 2004, she joined the Department of Information and Electrical Engineering (DIIIE), University of Salerno. Her research interests include digital signal processing and image-based measurement systems, measurement characterization, and instrument fault detection and isolation.

Alfredo Paolillo (M'08) was born in Belvedere Marittimo, Italy, in 1972. He received the M.S. degree in electronic engineering and the Ph.D. degree in information engineering from the University of Salerno, Salerno, Italy, in 2000 and 2004, respectively.

He is currently an Assistant Professor of electronic measurements with the Department of Information and Electrical Engineering (DIIIE), University of Salerno. His current research interests include optical fiber sensors and image-based and digital signal processing-based measurement systems.